ACS APPLIED ENERGY MATERIALS

Open Access

This article is licensed under CC-BY 4.0

www.acsaem.org

Article

On the Role of Boron-Engineered MWCNTs as Bifunctional Oxygen Evolution/Reduction Electrocatalysts

Giulia Tuci,*,# Marco Etzi,*,# Ida Ritacco,# Lorenzo Poggini, Andrea Rossin, Lucia Caporaso,* and Giuliano Giambastiani*

Cite This: *ACS Appl. Energy Mater.* 2026, 9, 11659−11668

Read Online

ACCESS | Metrics & More | Article Recommendations | Supporting Information

ABSTRACT: Oxygen reduction reaction (ORR) and oxygen evolution reaction (OER) represent key processes underpinning fuel cell and water-splitting technologies, respectively. In this scenario, boron-doped carbon nanomaterials have emerged as promising and metal-free bifunctional systems to promote both electrochemical processes while offering a sustainable alternative to the use of critical raw materials in electrocatalysts of the *state-of-the-art*. Herein, we describe the surface engineering of pristine multiwalled carbon nanotubes (MWCNTs) through the covalent grafting of precise boronic acid [R-B(OH)$_2$] or boronic ester [R-B(OR')$_2$] functionalities, using an aryl-diazonium salt method. Materials were then evaluated as ORR and OER electrocatalysts under alkaline conditions uncovering clear-cut structure–activity relationships commonly overlooked in the literature. DFT simulations on modeled boron-functionalized graphene systems unveiled the role of structural energetics linked to the dynamic evolution of B-active sites [R-B(OH)$_2$ *vs* R-B(OR')$_2$] under both electrochemical processes.

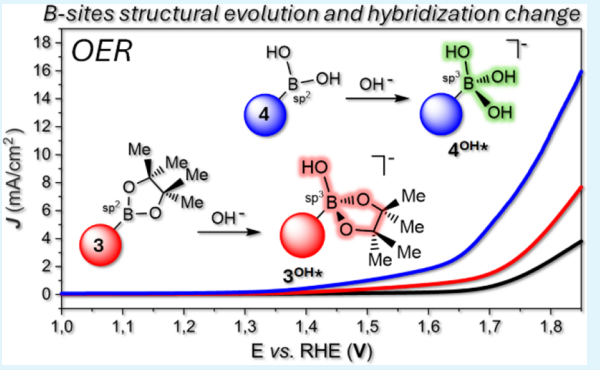

KEYWORDS: *carbon nanotube surface engineering, boron doping, oxygen evolution/reduction electrocatalysts, non-metal active site structural evolution*

1. INTRODUCTION

Oxygen reduction reaction (ORR) and oxygen evolution reaction (OER) have emerged as pivotal electrochemical processes for advancing sustainable energy technologies.[1−3] While the former is fundamental in fuel cell devices, the latter is decisive for enabling efficient water splitting and sustainable green hydrogen production.[4−6] High costs and limited natural abundance of critical transition metals used in electrocatalysts of the *state-of-the-art* for ORR (*i.e.*, Pt) and OER (*i.e.*, RuO_2/IrO_2)[1,7−12] have deeply hindered the large-scale implementation of these technologies. Over the past decade, metal-free carbocatalysts, prevalently in the form of lightweight hetero-doped materials (*i.e.*, N, O, B, P, and S), have emerged as powerful and stable alternatives to traditional metal-based systems. They are effective promoters in several thermal processes[13−18] as well as promising, low-cost substitutes for platinum-group metals (PGM) in fundamental electrocatalytic transformations at the heart of renewable energy technology.[19−28] In this scenario, B-doped materials have emerged as valuable bifunctional catalysts to promote ORR and OER.[3,29−31] The rational design of high-performance B-doped networks for both electrochemical processes remains contingent upon the control of the structural, electronic, and chemical environment of B-active sites. However, conventional methodologies applied to the bottom-up nanostructuring of complex (often batch-dependent) macromolecular C,B-networks (*i.e.*, hydrothermal treatment,[30,32,33] chemical vapor deposition,[34,35] and thermal annealing)[29,36,37] afford negligible control (if not a complete lack thereof) on the local structure and composition of B-active sites. On the contrary, they produce materials hosting a complex set of boron-containing species (*e.g.*, BC_3, B_4C, C-BO_2, B_2O_3, and C_2BO) whose heterogeneity hampers any reliable attempt to link materials electrochemical performance with a specific B-containing functional group.

Nevertheless, BC_3 groups have frequently been regarded as active species to promote the complete 4e$^-$ ORR,[30,33,38,39] while oxygen-enriched B-moieties (*e.g.*, C-BO_2 and/or C_2BO) preferentially boost the 2e$^-$ ORR path to form peroxide.[32,40−43] There are few reports on boron-doped carbon networks as metal-free electrocatalysts for the OER, and the identity of

Received: June 1, 2026
Revised: August 17, 2026
Accepted: August 21, 2026
Published: August 30, 2026

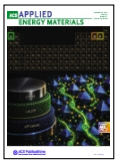

Downloaded from pubs.acs.org/aaemcq/article-pdf/9/17/11659/6792706/ae-2026-01791j.pdf by UNIV DEGLI STUDI DI FIRENZE user on 14 September 2026

© 2026 The Author(s). Published by American Chemical Society

https://doi.org/10.1021/acsaem.6c01791
ACS Appl. Energy Mater. 2026, 9, 11659−11668

their active sites still remains unclear.[3,29,30,44] While a theoretical study by Liu's group identified edge-type BC_3 moieties as promising candidates for high OER activity,[44] Choi and coworkers demonstrated experimentally that BCO_2 sites were more favorable for the adsorption and conversion of OH^- ions into O_2.[30]

In this work, we introduce an unconventional strategy to the synthesis of boron-decorated carbon nanomaterials. The approach is designed to clarify the role of specific B-containing functionalities in ORR and OER processes, circumventing limitations of heterogeneity of classical materials from bottom-up syntheses. A major advantage of our design method is that B-sites fall within consistent molecular frameworks and share identical structural and chemical environments at odds with those synthesized through classical bottom-up synthetic schemes.[45,46] To this end, precise boron-containing molecular fragments were covalently grafted to the outer surface of ultrapure, pristine multiwalled carbon nanotubes (MWCNTs). A mild, aryl-diazonium salt chemistry-based, top-down method enabled this functionalization preserving key chemico-physical properties of the hosting carbon matrix (*e.g.*, electrical conductivity, type and density of topological defects) and surface chemistry of B-functionalities essential to electrocatalytic runs. The study has uncovered a (previously unknown) distinct reactivity trend among structurally related boron functionalities. We find that boronic ester groups [R-B(OR′)$_2$] are highly active functionalities in the oxygen reduction reaction (ORR), in contrast to boronic acids [R-B(OH)$_2$], which are more effective in the oxygen evolution reaction (OER). DFT calculations on modeled graphene supercells functionalized with phenylboronic acid [ArB(OH)$_2$] or its pinacol ester (ArBpin) have finally offered a rationale to electrochemical results. They have unlocked the contribution of energetics linked to the dynamic structural evolution[47] of B-active sites as a critical factor in the catalytic performance of these metal-free systems. Only recently, Wu and coworkers demonstrated, using an oxygen-modified and defective graphene network, how dynamic evolutions of active sites were crucial to the function of carbon-based catalysts.[48] This previously overlooked characteristic, which is deemed even unmeasurable in B-groups embedded within bottom-up synthesized materials, is the key to understanding the mechanism of action of these lightweight doped samples in small-molecules activation and conversion.

2. EXPERIMENTAL SECTION

2.1. General Considerations

Unless otherwise stated, all material syntheses have been carried out using standard Schlenk-type techniques under N_2 atmosphere. *o*-DCB (*ortho*-dichlorobenzene) was dried following literature procedures,[26] while dry acetonitrile (CH_3CN) was obtained by means of an MBraun Solvent Purification System. All other solvents used throughout synthetic steps were degassed under N_2 atmosphere prior to any use and employed as received by the providers without undergoing any further purification. Multiwalled carbon nanotubes (MWCNTs, >98% in C—Lot no. MKBH5814V) and all other chemicals were purchased from Merck and used as received. An Elma S15 Elmasonic sonicator bath (37 kHz) was used for material sonication while their vacuum filtration during the workup procedure was accomplished using PTFE Whatman filters (0.2 μm pore size).

2.2. Covalent Grafting of B-Containing Functional Groups on Ultrapure MWCNT Samples

Material functionalization was accomplished following classical aryldiazonium salt chemistry.[14,24] In brief, 40 mg of ultrapure MWCNTs were suspended in either dry and degassed *o*-DCB (32 mL) or Milli-Q water (20 mL) and sonicated for 20 min before being treated with the proper aniline sample to get materials **3** and **4**, respectively. Afterward, each suspension was treated with aniline **1** (0.19 g, 0.86 mmol, in 16 mL of dry acetonitrile) and isopentyl nitrite (0.17 mL, 1.29 mmol) or aniline **2** (0.15 g, 0.86 mmol) and $NaNO_2$ (0.09 g, 1.29 mmol), respectively, and suspensions were sonicated for 10 min at room temperature. Each mixture was then stirred at 80 °C for 14 h during which surface functionalization takes place. After allowing mixtures to cool down at room temperature, each solid was recovered by centrifugation and submitted to successive washing/sonication/centrifugation cycles with ethyl acetate (twice) and dichloromethane (twice) for **3**, ethanol (four times) for **4**. Last, each solid was resuspended in proper solvent (CH_2Cl_2 for **3** and C_2H_5OH for **4**), sonicated for 10 min, and vacuum-filtered using Whatman filters (0.2 μm pore size). Recovered solid materials were then dried at 50 °C overnight and stored into a glass vial under ambient atmosphere without showing any appreciable alteration/decomposition over months. Blank samples for each functionalized material were prepared following identical synthetic and purification/workup procedures except for the use nitrite as an aniline activator.

2.3. Characterization Techniques

Thermogravimetric analysis (TGA) was carried out on an EXSTAR Seiko 6200 analyzer under N_2 atmosphere (100 mL/min). Analysis conditions were as follows: from 40 to 750 °C, 5 °C/min. X-ray photoelectron spectroscopy (XPS) was performed in an ultra-high vacuum system (10^{-9}–10^{-10} mbar) equipped with a non-monochromatized dual anode (Al and Mg) and a hemispherical electron/ion energy analyzer. The Al X-ray source was set at 120 W (12 kV and 10 mA) and photoelectrons collected normal to the sample surface, maintaining the analyzer angle at 54.5°. Each sample was suspended in ethanol and drop-cast on silicon wafer with native oxide. Samples were kept in the introduction chamber under vacuum for at least 18 h to remove all adsorbed volatiles and the solvent, with a base pressure in the order of 10^{-7} mbar. XPS spectra were acquired at a pass energy of 44.0 eV and elaborated using CasaXPS software.[49] Peak deconvolution was accomplished with Lorentzian functions and binding energy values calibrated at 284.8 eV (C 1s sp^2 component).[26] B 1s at % was estimated with a sensitivity factor of 0.159. Elemental analysis (EA) was performed on a Thermo Flash EA 1112 Series CHNS analyzer. Transmission electron microscopy (TEM) was carried out by means of a Thermo Fisher F200X G2 HR-TEM (200 keV beam energy). Samples were suspended in 2-propanol upon sonication and then deposited on holey-carbon-supported copper grids (200 mesh).

2.4. Electrochemical Measurements

Electrochemical measurements were conducted using a CHI760D potentiostat and an Ag/AgCl (3 M Cl^-) reference electrode. The electrolyte was a KOH (Merck, 84% min.) 0.1 M solution prepared using Milli-Q (18.2 MΩ·cm). An 85% *iR* correction was applied in all the electrochemical tests. All the potentials are reported *vs* reversible hydrogen electrode (RHE).

For the ink preparation, 1 mg of CNT was dispersed in a solution containing 136 μL of water, 88 μL of ethanol, and 4.8 μL of 5 wt % Nafion solution. The ink was sonicated until a homogeneous suspension was obtained. A proper ink volume was then deposited on the working electrodes by the drop-casting technique to achieve a catalyst loading of 0.35 mg cm^{-2}.

ORR measurements were conducted using a rotating rink-disk electrode (RRDE) setup equipped with a glassy carbon disk (ø 4 mm) and a Pt ring. The electrode was rotated at 800 rpm for the acquisition of

Downloaded from pubs.acs.org/aaemcq/article-pdf/9/17/11659/6792706/ae-2026-01791j.pdf by UNIV DEGLI STUDI DI FIRENZE user on 14 September 2026

https://doi.org/10.1021/acsaem.6c01791
ACS Appl. Energy Mater. 2026, 9, 11659–11668

the electrochemical data. A graphite rod was used as a counter electrode. N_2 or O_2 gas was bubbled to evaluate the base currents and ORR currents, respectively. Linear sweep voltammetry (LSV) was acquired at a scan rate of 10 mV s^{-1}, while the Pt ring was kept at a fixed potential of 1.2 V. Methanol tolerance was assessed by injection of 2 mL of methanol into the cell (electrolyte volume: ~40 mL) while the sample was subjected to a chronoamperometry at 0.61 V under O_2 atmosphere.

OER measurements were conducted using a glassy carbon electrode (active area: 0.5 cm^2) and a Pt wire as working and counter electrodes, respectively. LSVs were acquired at a scan rate of 10 mV s^{-1}. Chronoamperometry was conducted at 1.7 V. Tafel plots were derived from step chronoamperometry at increasing potentials in 20 mV steps. Each potential was held for 30 s, and the current density measured at the end of each step was plotted *vs* the overpotential (η) to construct the Tafel plot. Mass activities values (Table S3) were extracted from the LSV considering the catalyst loading on the electrode.

2.5. Computational Details

DFT calculations were performed using the Quantum Expresso code[50] employing the Perdew–Burke–Ernzerhof (PBE) exchange-correlation functional based on the generalized gradient approximation (GGA)[51] and ultrasoft pseudopotentials.[52] The spin-polarized Kohn–Sham equations were solved in the planewave pseudopotential framework, with the wavefunction basis set and the Fourier representation of the charge density being limited by kinetic cutoffs of 50 and 500 Ry, respectively.

The calculations were performed using a stoichiometric 8 × 8 graphene (Gr) supercell, consisting of 128 carbon atoms, functionalized with phenylboronic acid pinacol ester (ArBpin) and phenylboronic acid ($ArB(OH)_2$), under basic electrolyte conditions. The optimized structures corresponding to the most stable geometries of chemically grafted aromatics to Gr monolayers—labeled as Gr@ArBpin [159 atoms, (**3***)] and Gr@$ArB(OH)_2$ [143 atoms, (**4***)]—are shown in Figure S1.

A vacuum separation of 25 Å along the *z*-direction was entered between consecutive monolayers to prevent mutual influence with the periodic images and allow all atoms in the supercell to fully relax during optimization. The graphene supercell (Gr) was used as a model of the outer MWCNT wall to reduce the computational cost, since preliminary calculations showed essentially identical OH^- adsorption energies for the functionalized SWCNTs, representative of the MWCNT structure and Gr models (Figure S2). The Brillouin zone integration was performed on the Γ point only, and a Gaussian smearing with a width of σ = 0.05 eV was used in the calculations. In all calculations, the long-range nonlocal effects, such as van der Waals (vdW) interactions, were considered by including the dispersion correction through the zero damping DFT-D3 method of Grimme.[53]

The adsorption energy of the organic ligands on the Gr monolayer was computed using eq 1:

$$E_{ads} = E_{Gr@ArBX} - (E_{Gr} + E_{ArBX}) \quad (1)$$

where $E_{Gr@ArBX}$ is the energy of the total systems in which phenyl boronic acid [$ArB(OH)_2$] and phenyl boronic acid pinacol ester [ArBpin] are adsorbed on the Gr surface, E_{Gr} is the energy of the 8 × 8 graphene support, and E_{ArBX} is the energy of the organic fragments in the gas phase.

For the intermediates Gr@ArBpin@OH and Gr@$ArB(OH)_2$@OH, we computed the deformation energy (E_{def}), which is the energy required to distort the interacting fragments from their optimized geometries to those adopted upon interaction, and the interaction energy (E_{int}), defined as the interaction energy between the deformed fragments. These quantities were evaluated to rationalize the catalytic reactivity in terms of both the geometrical features and the bonding capabilities of the systems toward the adsorbate.[54]

The atom charges of the optimized **3*** and **4*** were computed by using the Bader's theory.[55−57]

The free energy diagrams of the universal OH intermediate descriptor along the electrochemical reaction pathway were computed using the computational hydrogen electrode (CHE) model developed by Nørskov et al.[58]

According to this model, under experimental conditions of pH = 13 and U = 1.23 V, where U is the applied electrochemical potential, the free energy of the ($H^+ + e^-$) pair is set equal to one-half of the chemical potential of gas-phase H_2.

The difference between the free energies of the initial and final states is computed using eq 2:

$$\Delta G = \Delta E + \Delta ZPE - T\Delta S - neU + nk_b T\ln 10 \times pH \quad (2)$$

where ΔE corresponds to the reaction energy obtained through DFT calculations, ZPE is the zero-point energy, S is the entropy, and T is the room temperature (298.15 K). In $-neU$, e is the elementary charge transferred and n is the number of proton–electron pairs transferred, whereas in $nk_bT\ln 10 \cdot pH$, k_b is the Boltzmann constant.

For both ORR and OER, the theoretical overpotential ($\eta^{ORR/OER}$) is defined according to eq 8 ($\eta^{ORR/OER} = U_0 - U_L$; *vide infra* Section 3). U_L, which is the ΔG_{max} of the whole processes, depends on the binding energy between the OH^- ion and the graphene support. Therefore, eqs 3 and 4

$$\Delta G_{maxORR} = -\Delta G_{*OH} \quad (3)$$

$$\Delta G_{maxOER} = \Delta G_{*OH} \quad (4)$$

will be the only descriptors to predict the ORR/OER catalyst activity.[59]

Quantum mechanics (QM) calculations were carried out using the Gaussian16 package.[60] The B3LYP-D3(BJ)[53,61] level of theory was used to optimize all geometries, and the 6-31G* basis set was used for C, H, O, and B atoms. In Figure S3, we reported the electronic and free energies (ΔE and ΔG) in both gas and solvent phases (in round brackets). In solvent, the free energies were obtained adding thermal corrections in the gas phase to the electronic energy computed via single-point energy calculations in water (polarizable continuum model)[62] at the B3LYP-D3(BJ) level[53,61] and using the 6-311G** basis set for all atoms.

3. RESULTS AND DISCUSSION

Two novel B-decorated MWCNTs have been prepared according to a slightly modified protocol based on classical aryldiazonium salt chemistry.[31] To this end, a sonicated suspension of ultrapure MWCNTs (98% C, Merck) was reacted with *in situ* generated aryl-diazonium salts from 4-aminophenylboronic acid pinacol ester (**1**) or 4-aminophenylboronic acid hydrochloride (**2**) in the presence of isopentyl nitrite or $NaNO_2$ as activator, respectively (Scheme 1).

Each sample underwent a thorough workup procedure involving sequential sonication/centrifugation cycles, followed by filtration and drying, to eliminate excess reagents and nonspecifically adsorbed (physiosorbed) molecules (detailed in Section 2). To rule out contamination from superficially adsorbed boron compounds, blank tests were conducted. For the latter, synthetic and workup procedures similar to those described for **3** and **4** were followed, but without the aniline activator.

The successful grafting of aryl groups was first assessed by thermogravimetric analyses (TGA), which showed distinctive weight losses for both functionalized materials (Figure 1A,B). The functional loading was tentatively estimated from the

Downloaded from pubs.acs.org/aaemcq/article-pdf/9/17/11659/6792470/ae-2026-01791j.pdf by UNIV DEGLI STUDI DI FIRENZE user on 14 September 2026

https://doi.org/10.1021/acsaem.6c01791
ACS Appl. Energy Mater. 2026, 9, 11659−11668

Scheme 1. Exohedral Functionalization Scheme of MWCNTs with Phenyl Boronic Acid Pinacol Ester (MW-Bpin, 3) or Phenyl Boronic Acid (MW-B(OH)$_2$, 4) Dangling Arms

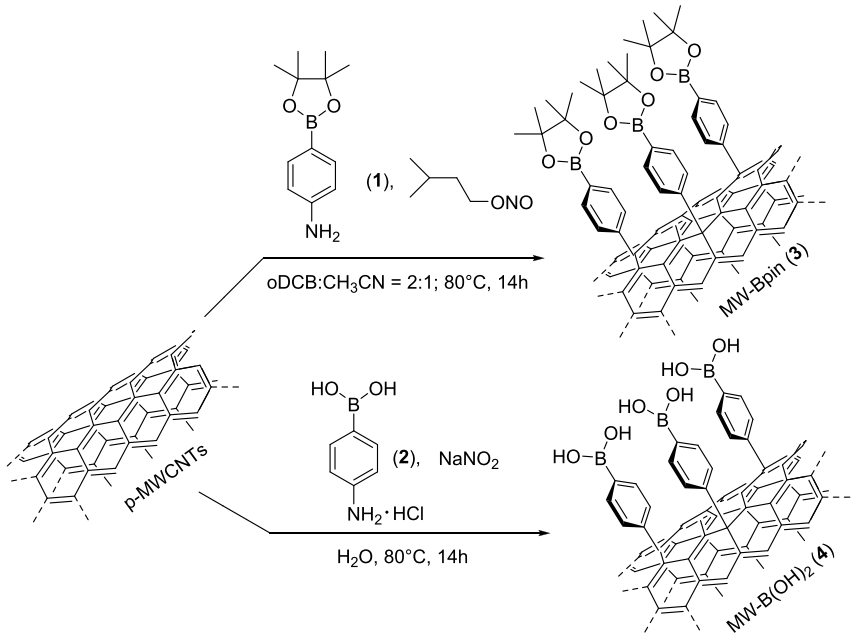

differential weight loss of each sample relative to its *blank counterpart* in the 40–500 °C temperature range (0.17 and 0.24 mmol/g for samples **3** and **4**, respectively). The moderate functionalization loading measured was ascribed to boron substituents on the aromatic rings. Their strong π–electron acceptor character stabilizes aryl radical intermediates generated upon reaction and decreases their reactivity to MWCNT surface grafting.[31,63] XPS analysis of **3** and **4** (Figure 1C,C′,D,D′) confirmed the successful functionalization procedure. While C 1*s* spectra revealed low-binding-energy components (283.6–283.7 eV), indicative of B–C bonds not detected in the control sample (*blank test*, Figure S4B), B 1*s* core regions showed signals at 190.9–191.0 eV from pinacol phenylboronic ester and boronic acid groups (Figure 1C′,D′).[30,64] No signals were detected from the high-resolution XPS analysis at the B 1*s* core region for the respective control samples (*blank tests*, Figure S4A). The boron loadings estimated from XPS analysis were 0.18 at. % (0.14 mmol/g) for **3** and 0.34 at. % (0.26 mmol/g) for **4**, in good agreement with TGA outcomes. A systematic characterization suite, including BET (Brunauer–Emmett–Teller) measures of material-specific surface areas, BJH (Barrett–Joyner–Halenda) analyses of their pore-size distribution/volume, Raman spectroscopy, and high-resolution TEM (transmission electron microscopy) micrographs of all materials, was finally employed to evaluate the morphological changes in MWCNT-based samples upon top-down functionalization paths. All collected characterization data (Figure 1E–J) were consistent with a highly conservative grafting technology for the surface exposure of tailored B-containing functional groups while preserving the unaltered morphology and composition of the underlying materials (MWCNTs). In particular, the invariance of the I_D/I_G ratio from the Lorentzian-fitted D (≈ 1360 cm^{-1}) and G (≈ 1590 cm^{-1}) peaks of Raman profiles (Figure 1G) indicates a constant and comparable level of structural defects relative to the well-ordered sp^2 graphitic domains in all samples.[65,66] TEM imaging (Figure 1H–J) reaffirms the noninvasive approach of surface grafting that preserves pristine CNT physical properties (*e.g.*, tube length and diameter) and nanotube bundling/aggregation degree in all functionalized materials.[24,26]

Samples **3** and **4**, including pristine multiwalled carbon nanotubes (MWCNTs), were then tested as electrocatalysts under alkaline conditions for the oxygen reduction reaction (ORR) and oxygen evolution reaction (OER). ORR performance was assessed in a three-electrode cell on a glassy carbon rotating ring-disk electrode (RRDE). Linear sweep voltammograms (LSVs) were recorded at a rotation rate of 800 rpm under both inert (N_2) and O_2-saturated 0.1 M KOH solution. As Figure 2A shows, all materials exhibit distinctive cathodic currents in the presence of O_2 not shown upon acquisition under inert (N_2) atmosphere (Figure S5), indicative of their ORR activity. Both boron-functionalized samples exhibit a positive shift in onset potential (E_{on}) compared to their pristine counterparts, with MW-Bpin (**3**) showing the best performance of the series (Figure 2 and Table 1). Despite a moderate B-group functional loading, with an onset potential (E_{on}) of 0.86 V and a half-wave potential ($E_{1/2}$) of 0.67 V, MW-Bpin (**3**) ranks among the best-performing B-doped, metal-free ORR catalysts reported in the literature to date (Table S1). It also exhibits complete tolerance to methanol poisoning/deactivation attempt, a critical issue for ORR electrocatalysts in direct methanol fuel cells.[67] This is demonstrated by its stable chronoamperometric response at 0.61 V, which remains virtually unaltered upon alcohol addition to the electrochemical cell (Figure S6).

ORR selectivity (2e$^-$ *vs* 4e$^-$) for electrocatalysts from this series was assessed by monitoring the hydrogen peroxide produced at the disk and intercepted at the Pt ring of the RRDE electrode (Figure 2A′). All materials exhibited a dominant four-electron process, with both B-functionalized samples

https://doi.org/10.1021/acsaem.6c01791
ACS Appl. Energy Mater. 2026, 9, 11659–11668

Downloaded from pubs.acs.org/aaemcq/article-pdf/9/17/11659/6792470/ae-2026-01791j.pdf by UNIV DEGLI STUDI DI FIRENZE user on 14 September 2026

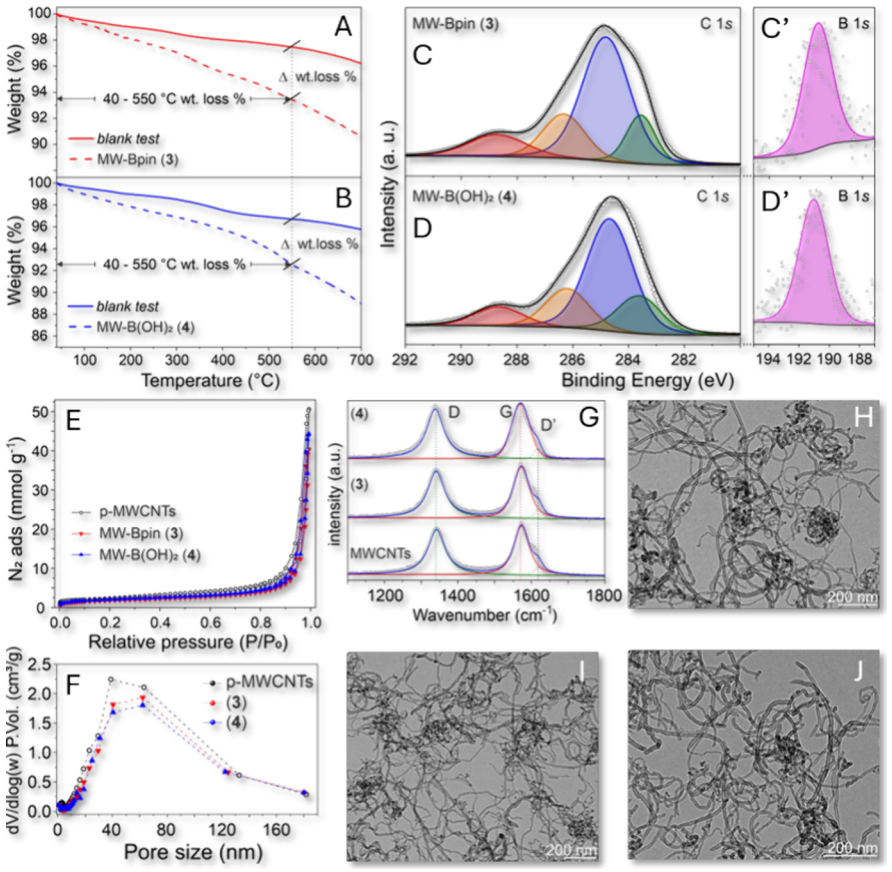

Figure 1. Thermogravimetric profiles of (A) MW-Bpin (**3**) and (B) MW-B(OH)$_2$ (**4**) and samples' weight loss *vs* their blank counterparts; analysis conditions: 40–750 °C, 5 °C/min, N_2 atm. (100 mL/min). High-resolution XPS profiles at the C 1*s* and B 1*s* core regions for (C, C′) MW-Bpin (**3**) and (D, D′) MW-B(OH)$_2$ (**4**) along with respective curve fitting. (E) N_2 adsorption–desorption isotherm linear plots of p-MWCNTs (black curve), **3** (red curve), and **4** (blue curve) recorded at 77 K along with their (F) respective pore-size distributions from the BJH method on N_2 desorption isotherm branches. (G) Raman spectra (empty gray dots) of p-MWCNTs, **3**, and **4**, fitted with Lorentzian line shapes (solid and dashed lines). TEM images of p-MWCNTs (H), **3** (I), and **4** (J) at comparable magnifications.

producing ∼10% of HO_2^- at 0.5 V, corresponding to an average of 3.8 electrons exchanged *per* O_2 molecule (Table 1).

Although the nature of the boron functional group (whether pinacol ester, **3**, or boronic acid, **4**) affects ORR kinetics (as evidenced by the shifting E_{on} values), it negligibly impacts the process selectivity ($4e^-$ *vs* $2e^-$). This key finding challenges the previously reported action of BCO_2 groups as ORR promoters for the selective $2e^-$ reduction pathway.[41,43]

Unlike complex, bottom-up synthesized boron-doped materials, our well-defined system unambiguously demonstrates that BCO_2 moieties (whatever acid or ester derivatives) promote ORR through a prevalent $4e^-$ reduction pathway while boronic esters [R-B(OR′)$_2$] exhibit superior O_2 activation kinetics than its acidic counterparts [R-B(OH)$_2$] (Figure 2 and Table 1, MW-Bpin, **3**, *vs* MW-B(OH)$_2$, **4**).

The oxygen evolution reaction (OER) performance of **3** and **4** was finally evaluated upon acquiring LSVs in a three-electrode cell in 0.1 M KOH electrolyte (Figure 2B). Unlike ORR activity trends of B-functionalized systems from this series, compound MW-B(OH)$_2$ (**4**) shows higher performance for the OER, with an E_{on} value of 1.6 V *vs* RHE and a remarkably high current density (η_{10} = 1.78 V *vs* RHE). With a relatively low concentration of surface grafted boronic acid groups, **4** significantly outperforms both its ester analogue MW-Bpin (**3**) and pristine MWCNTs and deservedly lies among the best boron-doped carbon-based OER electrocatalysts reported to date (Table S2). It also exhibits significant long-term stability under the scrutinized electrochemical conditions, as evidenced by its chronoamperometric response at 1.7 V *vs* RHE (Figure 2C). As shown in Figure S7, the Tafel plot obtained for MW-B(OH)$_2$ (**4**) was 126 mV dec^{-1}, a value typical of a first-electron rate-determining step in the OER kinetics. Tafel slopes for MWCNTs are strongly dependent on the OH^- concentration, as higher concentrations lead to lower slopes and faster kinetics.[68]

These findings provide original insights into the comprehension of the puzzling structure–activity and selectivity relationships of a significant class of metal-free electrocatalysts. Indeed, at odds to classical bottom-up synthesized and highly heterogeneous carbon structures where the chemical state, hybridization, and coordination of the boron dopants are poorly defined and uncontrollable, our top-down functionalization approach allows us to introduce a chemically, structurally, morphologically well-defined and uniform B-active species onto MWCNTs. Besides establishing the bifunctional catalytic aptitude for ORR/OER of selected B-containing functionalities, experimental data unambiguously demonstrate the non-innocent role of local C-BO_2 chemical environment and how

Downloaded from pubs.acs.org/aaemcq/article-pdf/9/17/11659/6792706/ae-2026-01791j.pdf by UNIV DEGLI STUDI DI FIRENZE user on 14 September 2026

https://doi.org/10.1021/acsaem.6c01791
ACS Appl. Energy Mater. 2026, 9, 11659−11668

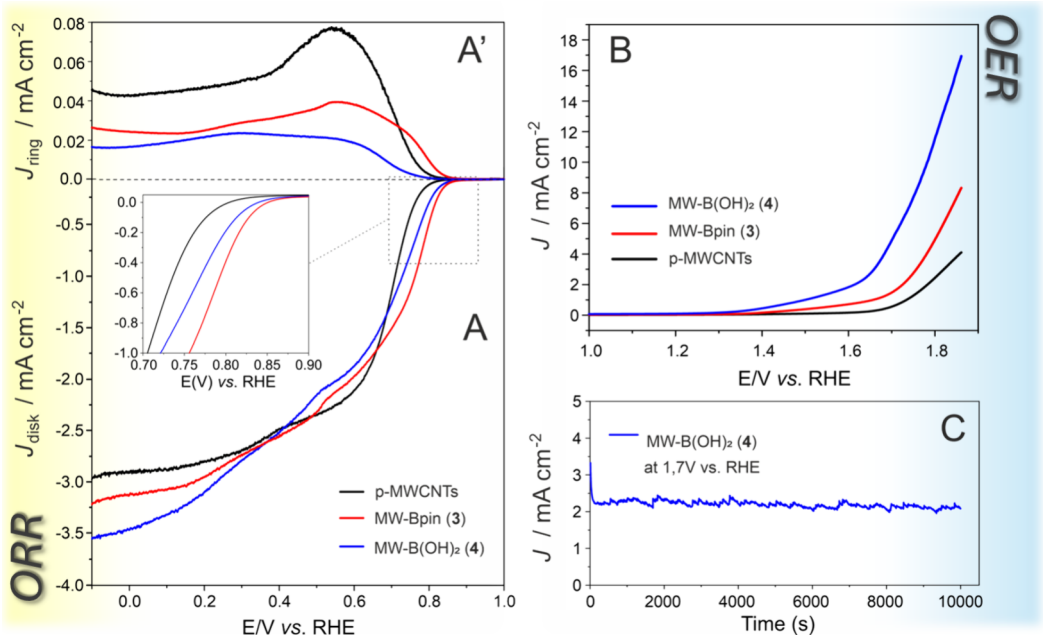

Figure 2. (A) Disk and (A') Pt-ring RRDE LSV curves of p-MWCNTs, **3**, and **4** registered in O_2-saturated 0.1 M KOH aqueous solution at an electrode spin rate of 800 rpm. (B) LSV polarization curves recorded for p-MWCNTs, **3**, and **4** at 10 mV/s in KOH 0.1 M solution. (C) Chronoamperometric response of MW-B$(OH)_2$ (**4**) at 1.7 V *vs* RHE.

Table 1. Onset Potential Values (E_{on}), H_2O_2 (%) Produced, and Mean Electron Number Exchanged (n) *per* O_2 Molecule for p-MWCNTs, 3, and 4

electrocatalyst	E_{on}	H_2O_2(%)[a]	n[a]
p-MWCNTs	0.79	21	3.6
MW-Bpin (**3**)	0.86	12	3.8
MW-B$(OH)_2$ (**4**)	0.83	9	3.8

[a]As measured from Pt-ring currents at 0.5 V.

it plays a decisive effect on the ultimate materials performance. A key finding concerns the dynamic structural evolution of boron-active sites, a previously overlooked feature that critically impacts the ultimate electrocatalytic efficiency of these metal-free systems. To clarify the concept, we conducted DFT computational studies primarily aimed at clarifying reasons why boronic acids [R-B$(OH)_2$] outperformed boronic ester groups [R-B$(OR')_2$] in OER. To this end, stoichiometric 8 × 8 graphene (Gr) supercells consisting of 128 carbon atoms, functionalized with pinacol ester [Gr@ArBpin; **3***] or phenylboronic acid [Gr@ArB$(OH)_2$; **4***] dangling groups were modeled and optimized (Figure S1), to calculate energetics of relevant intermediates involved in the process. Following the Nørskov approach, we calculated the ΔG associated with OH^- adsorption on the B sites of **3*** and **4***, as this step serves as the universal descriptor governing both electrochemical dissociative pathways (eqs 5a,c for ORR and eqs 6a,c for OER), as further detailed in Section 2.5.[46,59]

ORR dissociative pathway[69]

$$O_2 + H_2O + 2\,e^- + * \rightarrow O^* + 2\,OH^- \quad (5a)$$

$$O^* + H_2O + e^- \rightarrow OH^* + OH^- \quad (5b)$$

$$OH^* + e^- \rightarrow OH^- + * \quad (5c)$$

OER dissociative pathway[70]

$$OH^- + * \rightarrow OH^* + e^- \quad (6a)$$

$$OH^* + OH^- \rightarrow O^* + H_2O + e^- \quad (6b)$$

$$O^* + 2\,OH^- \rightarrow O_2 + H_2O + 2\,e^- + * \quad (6c)$$

The equations above show the oxygen reduction reaction (ORR; eqs 5a,c) and oxygen evolution reaction (OER; eqs 6a,c) dissociative pathways under alkaline electrolyte conditions.

Computed adsorption energy values (E_{ads}; eq 7) and Gibbs free energy variations (ΔG, eV) on intermediates Gr@ArBpin@OH ($\mathbf{3}^{\mathbf{OH}*}$) and Gr@ArB$(OH)_2$@OH ($\mathbf{4}^{\mathbf{OH}*}$) (eqs 5b and 6a) offered a first clear distinction on the stability of OH^- adsorbed species at the electron-deficient boron sites of DFT-optimized structures.

$$E_{ads} = E_{Gr@ArBX@OH\ (3^*/4^*)} - (E_{Gr@ArBX\ (3/4)} + E_{OH}) \quad (7)$$

where $E_{Gr@ArBX@OH\ (3*/4*)}$ and $E_{Gr@ArBX(3/4)}$ refer to the energy of intermediates resulting from the OH^- adsorption on **3** and/or **4** and energy of catalysts **3** and **4**, respectively; E_{OH} is the energy of the OH^- ion in the gas phase.

Adsorption energy (E_{ads}) values of −1.6 and −1.4 eV have finally been calculated for $\mathbf{3}^{\mathbf{OH}*}$ and $\mathbf{4}^{\mathbf{OH}*}$, respectively (Figure 3), with negative E_{ads} values denoting stable adsorption states. Furthermore, the Gibbs free energy variation (ΔG), calculated at an applied potential of 1.23 V (pH 13) according to the experimental conditions (see Section 2.5), showed that OH^- adsorption was thermodynamically favored on $\mathbf{3}^{\mathbf{OH}*}$ by

https://doi.org/10.1021/acsaem.6c01791
ACS Appl. Energy Mater. 2026, 9, 11659−11668

Downloaded from pubs.acs.org/aaemcq/article-pdf/9/17/11659/6792706/ae-2026-01791j.pdf by UNIV DEGLI STUDI DI FIRENZE user on 14 September 2026

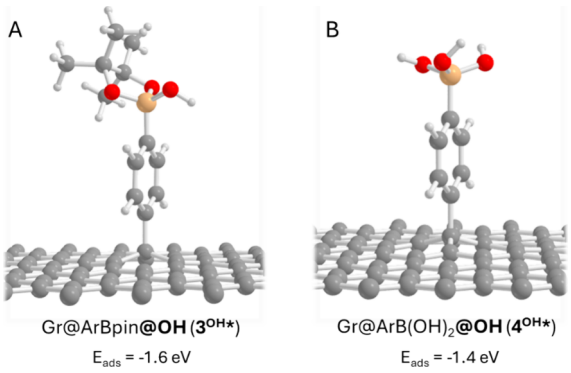

Figure 3. Optimized (graphically resized) structures of (A) Gr@ArBpin@OH ($\mathbf{3}^{OH*}$) and (B) Gr@ArB(OH)$_2$@OH ($\mathbf{4}^{OH*}$) intermediates associated with the respective calculated adsorption energies (E_{ads}, eV). Atoms color codes: C, light gray; H, white; O, red; B, orange.

approximately 0.2 eV compared to $\mathbf{4}^{OH*}$ (Figure S8). The performance of both catalytic species was further assessed by calculating the theoretical overpotential (η) for the oxygen evolution and reduction reactions (OER/ORR). This metric, $\eta^{ORR/OER}$ (eq 8), defined as the difference between the equilibrium potential (U_0 = 1.23 V) and the thermodynamic limiting potential ($U_L = \Delta G_{max}$), must be considered inversely proportional to the catalyst performance so that low η values signify high performance and *vice versa*.

$$\eta^{ORR/OER} = U_0 - U_L \quad (8)$$

where U_0 is the equilibrium potential (1.23 V) while U_L, also defined ΔG_{max}, is the thermodynamic limiting potential of the whole process (see Section 2.5).[59]

In accordance with ORR/OER experimental outcomes on **3** and **4** and the superior (computed) affinity of Gr@ArBpin (**3***) species to interact with the OH^- adsorbate than Gr@ArB(OH)$_2$ (**4***), catalyst **3*** exhibits better performance in ORR (η^{ORR} = 2.5 V) with respect to **4*** (η^{ORR} = 2.7 V) while an opposite trend was computed for the OER process [η^{OER} = –0.3 V *vs* –0.1 V for Gr@ArB(OH)$_2$ (**4***) and Gr@ArBpin (**3***), respectively].

Further analyses on the models have revealed distinctions between electronic and structural properties of boron-active sites. Based on Bader's theory,[55−57] we analyzed the charge of boron atoms in the DFT-optimized **3*** and **4*** models. Electronic structure analysis indicated a substantial lack of differentiation between B-sites (0.13e each), signifying that both of them (in **3*** and **4***) possessed similar Lewis acidity and electron-accepting capacity towards OH^- adsorbates. The main difference is of structural nature. Deformation energy (E_{def}) associated with the dynamic structural evolution of B-active sites in the transition from a trigonal planar (sp^2) to a tetrahedral (sp^3) geometry upon B atoms binding the OH^- adsorbate showed a lower value (1.8 eV) for **3*** → $\mathbf{3}^{OH*}$ transition than **4*** → $\mathbf{4}^{OH*}$ transition (2.4 eV). The higher deformation energy (E_{def}) in the latter was indicative of more pronounced distortion constraints around the B-site disfavoring B–OH bond formation. Further supporting this conclusion, the OH^-–B atom interaction energy (E_{int}) was slightly stronger on **4*** (–3.8 eV) than on **3*** (–3.4 eV). Despite this, the overall adsorption was less favorable for catalyst **4*** because a 0.4 eV gain in E_{int} did not compensate for the 0.6 eV higher deformation energy (ΔE_{def}). The Bpin moiety's rigidity imposes geometric constraints to **3*** that limit structural B-active site rearrangements upon OH^- binding, reducing deformation penalties and stabilizing the $\mathbf{3}^{OH*}$ intermediate (see also bond distances, angles, and dihedrals in Figure S9).

Therefore, the activity assessment of these metal-free systems requires considerations of both the chemical surroundings of C-BO_2 units and the dynamic structural evolution that B-active sites may undergo during electrochemical cycling. The proposed top-down synthetic approach (which introduces well-defined boron-containing functional groups) has unveiled fundamental reactivity features for these groups that are overlooked or even obscured in B-doped samples prepared by classical bottom-up schemes.

4. CONCLUSIONS

In this work, we report the case of a top-down surface engineering protocol (exohedral functionalization) for the decoration of ultrapure MWCNT samples with well-defined B-containing functionalities. We directly linked specific boron functional groups on carbon nanotubes to their catalytic performance in oxygen reduction/evolution reactions (ORR/OER). Key findings challenge the literature: generic BCO_2 groups (both ester or acid) boosted a prevalent $4e^-$ ORR pathway. Notably, boronic esters [R-B(OR′)$_2$] were superior to boronic acids [R-B(OH)$_2$] as ORR electrocatalysts ($E^3_{on} > E^4_{on}$), while the latter definitely outperformed in OER (E^4_{on}, $\eta^4_{10} > E^3_{on}$, η^3_{10}), where they ranked among the top-performing B-doped electrocatalysts for the process. These results underscore the critical and non-innocent role of local chemical environment of generic CBO_2 moieties, a factor overlooked from the literature to date.

DFT analyses on model 8 × 8 graphene (Gr) supercells functionalized with pinacol ester [Gr@ArBpin; **3***] or phenylboronic acid [Gr@ArB(OH)$_2$; **4***] dangling groups served to balance the interplay between stabilization and structural deformation energetics of OH^- adsorbate intermediates ($\mathbf{3}^{OH*}$ and $\mathbf{4}^{OH*}$) as common descriptors of both electrochemical processes. The stronger stabilization energy of $\mathbf{4}^{OH*}$ was not sufficient to compensate for the large energy penalty required to distort the boron site from trigonal planar (sp^2) to tetrahedral (sp^3). The overall less favorable OH^- adsorption energy explained the superior OER performance of the aryl-boronic acid functionalized materials. In **3***, the rigid Bpin framework minimized structural distortions upon OH^- binding, reducing energy penalties in stabilizing the intermediate $\mathbf{3}^{OH*}$ and ultimately enhancing its ORR activity.

In short, understanding the chemical and dynamic structural properties of active species throughout catalysis is a key prerequisite to uncover reaction mechanisms and guide to the design of high-performance, carbon-based metal-free electrocatalysts. Noteworthily, the top-down synthetic approach based on chemical functionalization can be easily applied to other heteroatoms beyond boron, hence significantly enlarging the impact of the present work.

■ ASSOCIATED CONTENT

Supporting Information

The Supporting Information is available free of charge at https://pubs.acs.org/doi/10.1021/acsaem.6c01791.

Downloaded from pubs.acs.org/aaemcq/article-pdf/9/17/11659/6792470/ae-2026-01791j.pdf by UNIV DEGLI STUDI DI FIRENZE user on 14 September 2026

https://doi.org/10.1021/acsaem.6c01791
ACS Appl. Energy Mater. 2026, 9, 11659−11668

(Figure S1) Optimized (computed) structures of Gr@ArBpin (**3***) and Gr@ArB$(OH)_2$ (**4***); (Figure S2) optimized (computed) structures of SWCNT@ArBpin@OH ($\mathbf{3^{OH*}}$) and SWCNT@ArB$(OH)_2$@OH ($\mathbf{4^{OH*}}$); (Figure S3) optimized geometries of the reduced models of the catalyst **3*** and **4*** and the intermediates; (Figure S4) high-resolution B 1s and C 1s XPS signals of the blank test; (Figure S5) LSV curves recorded in N_2 atmosphere; (Table S1) ORR performance of **3** and **4** at comparison with related materials from literature; (Figure S6) ORR chronoamperometric methanol tolerance response at 0.61 V *vs* RHE of MW-Bpin (**3**); (Table S2) OER performance of **4** at comparison with related materials from literature; (Figure S7) Tafel plot of MW-B$(OH)_2$ (**4**) for OER; (Table S3) mass activities toward OER at different potentials for MW-B$(OH)_2$ (**4**); equation to compute the Gibbs energy variations (ΔGs, eV) associated with OH-adsorbed intermediates; (Table S4) ZPE corrections for H_2 and H_2O gas phase species and ($\mathbf{3^{OH*}}$) and ($\mathbf{4^{OH*}}$) intermediates; (Table S5) entropy values of the H_2 and H_2O species at room temperature; (Figure S8) Gibbs energy variations (Δ*G*, eV) in the gas phase computed for Gr@ArBpin@OH ($\mathbf{3^{OH*}}$) and Gr@ArB$(OH)_2$@OH ($\mathbf{4^{OH*}}$) intermediates; (Figure S9) optimized structures of Gr@ArBpin (**3***) and Gr@ArB$(OH)_2$ (**4***) along with the corresponding OH-adsorbed intermediates (PDF)

AUTHOR INFORMATION

Corresponding Authors

Giulia Tuci – *Institute of Chemistry of OrganoMetallic Compounds, ICCOM-CNR and INSTM Unit, Via Madonna del Piano 10, Sesto Fiorentino, Florence 50019, Italy;* orcid.org/0000-0002-3411-989X; Email: giulia.tuci@iccom.cnr.it

Marco Etzi – *Center for Sustainable Future Technologies, Fondazione Istituto Italiano di Tecnologia, Via Livorno 60, Torino 10144, Italy;* orcid.org/0000-0001-7961-2138; Email: marco.etzi@iit.it

Lucia Caporaso – *Department of Chemistry and Biology "A. Zambelli", University of Salerno, Fisciano, Salerno 84084, Italy; CNR-IOM Democritos and International School for Advanced Studies (SISSA), Trieste 34136, Italy;* orcid.org/0000-0001-6623-3315; Email: lcaporaso@unisa.it

Giuliano Giambastiani – *Department of Chemistry "U. Schiff" (DICUS), University of Florence and INSTM Unit, Via della Lastruccia, 3-13, Sesto Fiorentino, Florence 50019, Italy; Institute of Chemistry of OrganoMetallic Compounds, ICCOM-CNR and INSTM Unit, Via Madonna del Piano 10, Sesto Fiorentino, Florence 50019, Italy;* orcid.org/0000-0002-0315-3286; Email: giuliano.giambastiani@unifi.it

Authors

Ida Ritacco – *Department of Chemistry and Biology "A. Zambelli", University of Salerno, Fisciano, Salerno 84084, Italy;* orcid.org/0000-0003-4392-9605

Lorenzo Poggini – *Institute of Chemistry of OrganoMetallic Compounds, ICCOM-CNR and INSTM Unit, Via Madonna del Piano 10, Sesto Fiorentino, Florence 50019, Italy; Department of Chemistry "U. Schiff" (DICUS), University of Florence and INSTM Unit, Via della Lastruccia, 3-13, Sesto Fiorentino, Florence 50019, Italy*

Andrea Rossin – *Institute of Chemistry of OrganoMetallic Compounds, ICCOM-CNR and INSTM Unit, Via Madonna del Piano 10, Sesto Fiorentino, Florence 50019, Italy*

Complete contact information is available at: https://pubs.acs.org/doi/10.1021/acsaem.6c01791

Author Contributions

[#]G.T., M.E., and I.R. equally contributed to the work. G.T., M.E., L.C., G.G.: conceptualization, methodology, data curation, writing—original draft, supervision, and funding acquisition. I.R., L.P., and A.R.: formal analysis, data curation, methodology, validation, writing—review and editing.

Notes

The authors declare no competing financial interest.

ACKNOWLEDGMENTS

The Italian MUR through PRIN2022 projects "MATISSE-2022K5SX27", "MULTIPOR-2022R5E2P5", "LUMIMOF-2022A3XNWJ", "MUSE-2022E5L4Y2", and the NextGeneration EU - POR H2 AdP MMES/ENEA (PNRR - Mission 2, Component 2, Investment 3.5, "Ricerca e sviluppo sull'idrogeno" (B93C22000630006) are kindly acknowledged for the financial support. L.C. acknowledges the Project PE0000021 "Network 4 Energy Sustainable Transition", by NextGeneration EU EINSTEIN for the financial support. Supercomputing Phoenix at Department of Chemistry and Biology "A. Zambelli", University of Salerno, Italy, is also acknowledged for providing computer time resources.

REFERENCES

(1) Su, G.; Yang, J.; Yin, J. Advancements in Electrocatalysts for Oxygen Evolution Reaction: A Review of Catalysts in Acidic Media. *ChemElectroChem* **2025**, *12*, No. e202400559.

(2) Alfaifi, S. M.; Balu, R.; Chiang, K.; Choudhury, N. R.; Dutta, N. K. Electrocatalysts for the Oxygen Reduction Reaction in Proton Exchange Membrane Fuel Cells: Significant Advances, Major Challenges, and Future Directions. *ACS Catal.* **2025**, *15*, 9301–9345.

(3) Vineesh, T. V.; Kumar, M. P.; Takahashi, C.; Kalita, G.; Alwarappan, S.; Pattanayak, D. K.; Narayanan, T. N. Bifunctional Electrocatalytic Activity of Boron-Doped Graphene Derived from Boron Carbide. *Adv. Energy Mater.* **2015**, *5*, No. 1500658.

(4) Zhao, T.; Wang, J.; Wei, Y.; Zhuang, Z.; Dou, Y.; Yang, J.; Li, W.-H.; Wang, D. From lab-scale to industrialization: atomically M–N–C catalysts for the oxygen reduction reaction. *Energy Environ. Sci.* **2025**, *18*, 3462–3501.

(5) Liang, Z.; Lei, H.; Zheng, H.; Wang, H.-Y.; Zhang, W.; Cao, R. Selective two-electron and four-electron oxygen reduction reactions using Co-based electrocatalysts. *Chem. Soc. Rev.* **2025**, *54*, 5248–5291.

(6) Ku, Y.; Zhang, K.; Guo, Y.; Chang, S.; Yan, Y.; Zheng, G.; Gao, H.; Song, D.; Yang, X.; Cheng, S.; Dong, L.; Shan, C. Boron-doped diamond composites for durable oxygen evolution. *J. Colloid Interface Sci.* **2025**, *677*, 675–682.

(7) Liu, Y.-X.; Zhang, W.-Y.; Han, G.-K.; Zhou, Y.-W.; Li, L.-F.; Kang, C.; Kong, F.-P.; Gao, Y.-Z.; Du, C.-Y.; Wang, J.-J.; Ma, Y.-L.; Du, L.; Cai, W.-B.; Yin, G.-P. Deactivation and regeneration of a benchmark Pt/C catalyst toward oxygen reduction reaction in the presence of poisonous SO_2 and NO. *Catal. Sci. Technol.* **2022**, *12*, 2929–2934.

Downloaded from pubs.acs.org/aaemcq/article-pdf/9/17/11659/6792470/ae-2026-01791j.pdf by UNIV DEGLI STUDI DI FIRENZE user on 14 September 2026

(8) Li, S.; Shi, L.; Guo, Y.; Wang, J.; Liu, D.; Zhao, S. Selective oxygen reduction reaction: mechanism understanding, catalyst design and practical application. *Chem. Sci.* **2024**, *15*, 11188–11228.
(9) Ferreira da Silva, C. D.; Claudel, F.; Chattot, V. M. R.; Abbou, S.; Kumar, K.; Jiménez-Morales, I.; Cavaliere, S.; Jones, D.; Rozière, J.; Solà-Hernandez, L.; Beauger, C.; Faustini, M.; Peron, J.; Gilles, B.; Encinas, T.; Piccolo, L.; Barros de Lima, F. H.; Dubau, L.; Maillard, F. Oxygen Evolution Reaction Activity and Stability Benchmarks for Supported and Unsupported IrO_x Electrocatalysts. *ACS Catal.* **2021**, *11*, 4107–4116.
(10) Pascuzzi, M. E. C.; Goryachev, A.; Hofmann, J. P.; Hensen, E. J. M. Mn promotion of rutile TiO_2-RuO_2 anodes for water oxidation in acidic media. *Appl. Catal., B* **2020**, *261*, No. 118225.
(11) Pascuzzi, M. E. C.; Hofmann, J. P.; Hensen, E. J. M. Promoting oxygen evolution of IrO_2 in acid electrolyte by Mn. *Electrochim. Acta* **2021**, *366*, No. 137448.
(12) Cardone, A. G.; Bartoli, M.; Sacco, A.; Pirri, C. F.; Etzi, M. Microwave-Assisted Synthesis of Ir—Ni Electrocatalystsfor the Oxygen Evolution Reaction in Acidic Electrolyte. *ChemistryOpen* **2025**, *14*, No. e202500279.
(13) Wu, S.; Yu, L.; Wen, G.; Xie, Z.; Lin, Y. Recent progress of carbon-based metal-free materials in thermal-driven catalysis. *J. Energy Chem.* **2021**, *58*, 318–335.
(14) Tuci, G.; Rossin, A.; Luconi, L.; Pham-Huu, C.; Cicchi, S.; Ba, H.; Giambastiani, G. Pyridine-Decorated Carbon Nanotubes as a Metal-Free Heterogeneous Catalyst for Mild CO_2 Reduction to Methanol with Hydroboranes. *Catal. Sci. Technol.* **2017**, *7*, 5833–5837.
(15) Feng, L.; Ali, S.; Xu, C.; Jiang, Q.; Tuci, G.; Giambastiani, G.; Pham-Huu, C.; Liu, Y. Assessing the Nature of Active Sites on Nanodiamonds as Metal-Free Catalysts for the EB-to-ST Direct Dehydrogenation Using a Catalytic Approach. *ACS Catal.* **2022**, *22*, 6119–6131.
(16) Duong-Viet, C.; Nhut, J.-M.; Truong-Huu, T.; Tuci, G.; Nguyen-Dinh, L.; Pham, C.; Giambastiani, G.; Pham-Huu, C. Tailoring Properties of Metal-Free Catalysts for the Highly Efficient Desulfurization of Sour Gases under Harsh Conditions. *Catalysts* **2021**, *11*, No. 226.
(17) Chen, S. S.; Carraher, J. M.; Tuci, G.; Rossin, A.; Raman, C. A.; Luconi, L.; Tsang, D. C. W.; Giambastiani, G.; Tessonnier, J.-P. Engineered Nitrogen-Decorated Carbon Networks for the Metal-Free Catalytic Isomerization of Glucose to Fructose. *ACS Sustain. Chem. Eng.* **2019**, *7*, 16959–16963.
(18) Duong-Viet, C.; Nhut, J.-M.; Truong-Huu, T.; Tuci, G.; Nguyen-Dinh, L.; Liu, Y.; Pham, C.; Giambastiani, G.; Pham-Huu, C. A nitrogen-doped carbon-coated silicon carbide as a robust and highly efficient metal-free catalyst for sour gas desulfurization in the presence of aromatics as contaminants. *Catal. Sci. Technol.* **2020**, *10*, 5487–5500.
(19) Zhai, Q.; Huang, H.; Lawson, T.; Xia, Z.; Giusto, P.; Antonietti, M.; Jaroniec, M.; Chhowalla, M.; Baek, J.-B.; Liu, Y.; Qiao, S.; Dai, L. Recent Advances on Carbon-Based Metal-Free Electrocatalysts for Energy and Chemical Conversions. *Adv. Mater.* **2024**, *36*, No. 2405664.
(20) Naz, R.; Tahir, M. Recent Developments in Metal-free Materials for Photocatalytic and Electrocatalytic Carbon Dioxide Conversion into Value Added Products. *Energy Fuels* **2025**, *39*, 6127–6150.
(21) Wei, S.; Lan, G.; Qiu, Y.; Lin, D.; Kong, W.; Li, Y. Advances in metal-free carbon catalysts for acetylene hydrochlorination: From heteroatom doping to intrinsic defects over the past decade. *Chin. J. Catal.* **2025**, *70*, 8–43.
(22) Tuci, G.; Rossin, A.; Saki, Z.; Caporaso, L.; Liu, Y.; Centi, G.; Giambastiani, G. The Still Elusive Role of Lightweight Doping in Carbon-Based Electrocatalysts for the Selective Oxygen Reduction Reaction to Hydrogen Peroxide. *ChemSusChem* **2024**, *17*, No. e202400660.
(23) Tuci, G.; Rossin, A.; Zhang, X.; Pham-Huu, C.; Giambastiani, G. Exohedrally functionalized carbon-based networks as catalysts for electrochemical syntheses. *Curr. Opin. Green Sustainable Chem.* **2022**, *33*, No. 100579.
(24) Tuci, G.; Zafferoni, C.; Rossin, A.; Milella, A.; Luconi, L.; Innocenti, M.; Truong Phuoc, L.; Duong-Viet, C.; Pham-Huu, C.; Giambastiani, G. Chemically Functionalized Carbon Nanotubes with Pyridine Groups as Easily Tunable N-Decorated Nanomaterials for the Oxygen Reduction Reaction in Alkaline Medium. *Chem. Mater.* **2014**, *26*, 3460–3470.
(25) Tuci, G.; Zafferoni, C.; D'Ambrosio, P.; Caporali, S.; Ceppatelli, M.; Rossin, A.; Tsoufis, T.; Innocenti, M.; Giambastiani, G. Tailoring Carbon Nanotube N-Dopants while Designing Metal-Free Electrocatalysts for the Oxygen Reduction Reaction in Alkaline Medium. *ACS Catal.* **2013**, *3*, 2108–2111.
(26) Tuci, G.; Rossin, A.; Zhang, X.; Truong Phuoc, L.; Berretti, E.; Liu, Y.; Pham-Huu, C.; Ali, S.; Jan, F.; Poggini, L.; Giambastiani, G. Metal-free Electrocatalysts for the Selective 2e- Oxygen Reduction Reaction: A Never-Ending Story? *Chem. – Eur. J.* **2023**, *29*, No. e202301036.
(27) Tuci, G.; Luconi, L.; Rossin, A.; Berretti, E.; Ba, H.; Innocenti, M.; Yakhvarov, D.; Caporali, S.; Pham-Huu, C.; Giambastiani, G. Aziridine-Functionalized Multiwalled Carbon Nanotubes: Robust and Versatile Catalysts for the Oxygen Reduction Reaction and Knoevenagel Condensation. *ACS Appl. Mater. Interfaces* **2016**, *8*, 30099–30106.
(28) Tuci, G.; Filippi, J.; Ba, H.; Rossin, A.; Luconi, L.; Pham-Huu, C.; Vizza, F.; Giambastiani, G. How to Teach an Old Dog New (Electrochemical) Tricks: Aziridine-Functionalized CNTs as Efficient Electrocatalysts for the Selective CO_2 Reduction to CO. *J. Mater. Chem. A* **2018**, *6*, 16382–16389.
(29) Cheng, Y.; Tian, Y.; Fan, X.; Liu, J.; Yan, C. Boron Doped Multiwalled Carbon Nanotubes as Catalysts for Oxygen Reduction Reaction and Oxygen Evolution Reactionin in Alkaline Media. *Electrochim. Acta* **2014**, *143*, 291–296.
(30) Tam, T. V.; Kang, S. G.; Kim, M. H.; Lee, S. G.; Hur, S. H.; Chung, J. S.; Choi, W. M. Novel Graphene Hydrogel/B-Doped Graphene Quantum Dots Composites as Trifunctional Electrocatalysts for Zn-Air Batteries and Overall Water Splitting. *Adv. Energy Mater.* **2019**, *9*, No. 1900945.
(31) Bahr, J. L.; Tour, J. M. Highly Functionalized Carbon Nanotubes Using *in Situ* Generated Diazonium Compounds. *Chem. Mater.* **2001**, *13*, 3823–3824.
(32) Ri, K. C.; Pak, S. S.; Sun, D.; Zhong, Q.; Yang, S.; Sin, S.; Wu, L.; Sun, Y.; Cao, H.; Han, C.; Xu, C.; Liu, Y.; He, H.; Li, S.; Sun, C. Boron-doped rGO electrocatalyst for high effective generation of hydrogen peroxide: Mechanism and effect of oxygen-enriched air. *Appl. Catal., B* **2024**, *343*, No. 123471.
(33) Tafoya, J. P. V.; Doszczeczko, S.; Titirici, M. M.; Sobrido, A. B. J. Enhancement of the electrocatalytic activity for the oxygen reduction reaction of boron-doped reduced graphene oxide via ultrasonic treatment. *Int. J. Hydrogen Energy* **2022**, *47*, 5462–5473.
(34) Sawant, S. V.; Patwardhan, A. W.; Joshi, J. B.; Dasgupta, K. Boron doped carbon nanotubes: Synthesis, characterization and emerging applications – A review. *Chem. Eng. J.* **2022**, *427*, No. 131616.
(35) Yang, L.; Jiang, S.; Zhao, Y.; Zhu, L.; Chen, S.; Wang, X.; Wu, Q.; Ma, J.; Ma, Y.; Hu, Z. Boron-Doped Carbon Nanotubes as Metal-Free Electrocatalysts for the Oxygen Reduction Reaction. *Angew. Chem., Int. Ed.* **2011**, *50*, 7132–7135.
(36) Lin, Y.; Zhu, Y.; Zhang, B.; Kim, Y. A.; Endo, M.; Su, D. S. Boron-doped onion-like carbon with enriched substitutional boron: the relationship between electronic properties and catalytic performance. *J. Mater. Chem. A* **2015**, *3*, 21805–21814.
(37) Pourazadi, E.; Haque, E.; Faisal, S. N.; Harris, A. T. Identification of electrocatalytic oxygen reduction (ORR) activity of boron in graphene oxide; incorporated as a charge-adsorbate and/or substitutional p-type dopant. *Mater. Chem. Phys.* **2018**, *207*, 380–388.
(38) Suo, N.; Huang, H.; Wang, X.; Hou, X.; Shao, Z.; Zhang, G. Facile synthesis and electrocatalytic performance for oxygen reduction of boron-doped carbon catalysts on graphene sheets. *Fuel Cells* **2021**, *21*, 328–336.
(39) Tam, T. V.; Kang, S. G.; Babu, K. F.; Oh, E.-S.; Lee, S. G.; Choi, W. M. Synthesis of B-doped graphene quantum dots as a metal-free

Downloaded from pubs.acs.org/aaemcq/article-pdf/9/17/11659/6792470/ae-2026-01791j.pdf by UNIV DEGLI STUDI DI FIRENZE user on 14 September 2026

electrocatalyst for the oxygen reduction reaction. *J. Mater. Chem. A* **2017**, *5*, 10537–10543.
(40) Kim, D. J.; Gao, Y.; Rigby, K.; Meese, A. F.; Lim, H. J.; Wang, H.; Kim, J. H.; Kim, J.-H. Pulsed Electrolysis of Boron-Doped Carbon Dramatically Improves Impurity Tolerance and Longevity of H_2O_2 Production. *Environ. Sci. Technol.* **2023**, *57*, 7309–7320.
(41) Byeon, A.; Choi, J. W.; Lee, H. W.; Yun, W. C.; Zhang, W.; Hwang, C.-K.; Lee, S. Y.; Han, S. S.; Kim, J. M.; Lee, J. W. CO_2-derived edge-boron-doped hierarchical porous carbon catalysts for highly effective electrochemical H_2O_2 production. *Appl. Catal. B: Environ.* **2023**, *329*, No. 122557.
(42) Xia, Y.; Zhao, X.; Xia, C.; Wu, Z.-Y.; Zhu, P.; Kim, J. Y.; Bai, X.; Gao, G.; Hu, Y.; Zhong, J.; Liu, Y.; Wang, H. Highly active and selective oxygen reduction to H_2O_2 on boron-doped carbon for high production rates. *Nat. Commun.* **2021**, *12*, No. 4225.
(43) Yun, W. C.; Yang, J.; Lee, D.; Lee, J.; Kim, J.; Byeon, A.; Lee, J. W. Enhanced electroproduction of hydrogen peroxide with oxidized boron-doped carbon catalysts synthesized from gaseous CO_2. *J. CO2 Util.* **2024**, *84*, No. 102833.
(44) Kong, X.; Huang, Y.; Liu, Q. Two-dimensional boron-doped graphyne nanosheet: A new metal-free catalyst for oxygen evolution reaction. *Carbon* **2017**, *123*, 558–564.
(45) Costentin, C.; Savéant, J.-M. Towards an intelligent design of molecular electrocatalysts. *Nat. Rev.* **2017**, *1*, No. 87.
(46) Xu, H.; Cheng, D.; Cao, D.; Zeng, X. C. A universal principle for a rational design of single-atom electrocatalysts. *Nat. Catal.* **2018**, *1*, 339–348.
(47) Chen, Z.-B.; Zhang, Y.-L.; Sun, Y.-T.; Wang, Y.-H.; Wan, Q.; Zhou, X.-S. Dynamic Structural Evolution of Active Sites and Effect on Heterogeneous Catalysis: Theoretical Insights. *Chem Asian J.* **2025**, *20*, No. e202401762.
(48) Wu, Q.; Zou, H.; Mao, X.; He, J.; Shi, Y.; Chen, S.; Yan, X.; Wu, L.; Lang, C.; Zhang, B.; Song, L.; Wang, X.; Du, A.; Li, Q.; Jia, Y.; Chen, J.; Yao, X. Unveiling the dynamic active site of defective carbon-based electrocatalysts for hydrogen peroxide production. *Nat. Commun.* **2023**, *14*, No. 6275.
(49) Fairley, N.; Fernandez, V.; Richard-Plouet, M.; Guillot-Deudon, C.; Walton, J.; Smith, E.; Flahaut, D.; Greiner, M.; Biesinger, M.; Tougaard, S.; Morgan, D.; Baltrusaitis, J. Systematic and collaborative approach to problem solving using X-ray photoelectron spectroscopy. *Appl. Surf. Sci. Adv.* **2021**, *5*, No. 100112.
(50) Giannozzi, P.; Andreussi, O.; Brumme, T.; Bunau, O.; Buongiorno Nardelli, M.; Calandra, M.; Car, R.; Cavazzoni, C.; Ceresoli, D.; Cococcioni, M.; Colonna, N.; Carnimeo, I.; Dal Corso, A.; de Gironcoli, S.; Delugas, P.; DiStasio, R. A. Jr.; Ferretti, A.; Floris, A.; Fratesi, G.; Fugallo, G.; Gebauer, R.; Gerstmann, U.; Giustino, F.; Gorni, T.; Jia, J.; Kawamura, M.; Ko, H.-Y.; Kokalj, A.; Küçükbenli, E.; Lazzeri, M.; Marsili, M.; Marzari, N.; Mauri, F.; Nguyen, N. L.; Nguyen, H.-V.; Otero-de-la-Roza, A.; Paulatto, L.; Poncé, S.; Rocca, D.; Sabatini, R.; Santra, B.; Schlipf, M.; Seitsonen, A. P.; Smogunov, A.; Timrov, I.; Thonhauser, T.; Umari, P.; Vast, N.; Wu, X.; Baroni, S. Advanced capabilities for materials modelling with Quantum ESPRESSO. *J. Phys.: Condens. Matter* **2017**, *29*, No. 465901.
(51) Perdew, J. P.; Burke, K.; Ernzerhof, M. Generalized Gradient Approximation Made Simple. *Phys. Rev. Lett.* **1996**, *77*, 3865–3868.
(52) Vanderbilt, D. Soft self-consistent pseudopotentials in a generalized eigenvalue formalism. *Phys. Rev. B* **1990**, *41*, No. 7892.
(53) Grimme, S.; Antony, J.; Ehrlich, S.; Krieg, H. A consistent and accurate ab initio parametrization of density functional dispersion correction (DFT-D) for the 94 elements H-Pu. *J. Chem. Phys.* **2010**, *132*,No. 154104.
(54) Falivene, L.; Kozlov, S. M.; Cavallo, L. Constructing Bridges between Computational Tools in Heterogeneous and Homogeneous Catalysis. *ACS Catal.* **2018**, *8*, 5637–5656.
(55) Henkelman, G.; Arnaldsson, A.; Jònsson, H. A Fast and Robust Algorithm for Bader Decomposition of Charge Density. *Comput. Mater. Sci.* **2006**, *36*, 354–360.
(56) Sanville, E.; Kenny, S. D.; Smith, R.; Henkelman, G. Improved Grid-Based Algorithm for Bader Charge Allocation. *J. Comput. Chem.* **2007**, *28*, 899–908.
(57) Tang, W.; Sanville, E.; Henkelman, G. A Grid-Based Bader Analysis Algorithm Without Lattice Bias. *J. Phys. Condens. Matter* **2009**, *21*, No. 084204.
(58) Nørskov, J. K.; Rossmeisl, J.; Logadottir, A.; Lindqvist, L.; Kitchin, J. R.; Bligaard, T.; Jònsson, H. Origin of the Overpotential for Oxygen Reduction at a Fuel-Cell Cathode. *J. Phys. Chem. B* **2004**, *108*, 17886–17892.
(59) Xu, H. H. H.; Cheng, D.; Cao, D.; Cheng Zheng, X. Revisiting the universal principle for the rational design of single-atom electrocatalysts. *Nat. Catal.* **2024**, *7*, 207–218.
(60) Frisch, M. J.; Trucks, G. W. Schlegel, H. B.; Scuseria, G. E.; Robb, M. A.; Cheeseman, J. R.; Scalmani, G.; Barone, V.; Petersson, G. A.; Na-katsuji, H.; Li, X.; Caricato, M.; Marenich, A. V.; Bloino, J.; Janesko, B. G.; Gomperts, R.; Mennucci, B.; Hratchian, H. P.; Ortiz, J. V.; Izmaylov, A. F.; Sonnenberg, J. L.; Williams, D.; Ding, F.; Lipparini, F.; Egidi, F.; Goings, J.; Peng, B.; Petrone, A.; Henderson, T.; Ranasinghe, D.; Zakrzewski, V. G.; Gao, J.; Rega, N.; Zheng, G.; Liang, W.; Hada, M.; Ehara, M.; Toyota, K.; Fukuda, R.; Hasegawa, J.; Ishida, M.; Nakajima, T.; Honda, Y.; Kitao, O.; Nakai, H.; Vreven, T.; Throssell, K.; Montgomery, J. A. Jr.; Per-alta, J. E.; Ogliaro, F.; Bearpark, M. J.; Heyd, J. J.; Broth-ers, E. N.; Kudin, K. N.; Staroverov, V. N.; Keith, T. A.; Kobayashi, R.; Normand, J.; Raghavachari, K.; Rendell, A. P.; Burant, J. C.; Iyengar, S. S.; Tomasi, J.; Cossi, M.; Millam, J. M.; Klene, M.; Adamo, C.; Cammi, R.; Ochter-ski, J. W.; Martin, R. L.; Morokuma, K.; Farkas, O.; Foresman, J. B.; Fox, D. J. *Gaussian 16*, Revision C.01; Gaussian, Inc., **2016**.
(61) Allouche, A.-R. Gabedit—A graphical user interface for computational chemistry softwares. *J. Comput. Chem.* **2011**, *32*, 174–182.
(62) Mennucci, B. T., J.; Cammi, R.; Cheeseman, J. R.; Frisch, M. J.; Devlin, F. J.; Gabriel, S.; Stephens, P. J. Polarizable Continuum Model (PCM) Calculations of Solvent Effects on Optical Rotations of Chiral Molecules. *J. Phys. Chem. A* **2002**, *106*, 6102–6113.
(63) Schmidt, G.; Gallon, S.; Esnouf, S.; Bourgoin, J.-P.; Chenevier, P. Mechanism of the Coupling of Diazonium to Single-Walled Carbon Nanotubes and Its Consequences. *Chem. – Eur. J.* **2009**, *15*, 2101–2110.
(64) Das, R. K.; Mohapatra, S. Highly luminescent, heteroatom-doped carbon quantum dots for ultrasensitive sensing of glucosamine and targeted imaging of liver cancer cells. *J. Mater. Chem. B* **2017**, *5*, 2190–2197.
(65) Ferrari, A. C.; Robertson, J. Interpretation of Raman spectra of disordered and amorphous carbon. *Phys. Rev. B* **2000**, *61*, 14095–14107.
(66) Lucchese, M. M.; Stavale, F.; Martins Ferreira, E. H.; Vilani, C.; Moutinho, M. V. O.; Capaz, R. B.; Achete, C. A.; Jorio, A. Quantifying ion-induced defects and Raman relaxation length in graphene. *Carbon* **2010**, *48*, 1592–1597.
(67) Tan, Y.; Xu, C.; Chen, G.; Zheng, N.; Xie, Q. A Graphene-Platinum Nanoparticles-Ionic Liquid Composite Catalyst for Methanol-Tolerant Oxygen Reduction. *Energy Environ. Sci.* **2012**, *5*, 6923–6927.
(68) Cheng, Y.; Kwofie, F.; Chen, Z.; Zhang, R.; Wang, Z.; Jiang, S. P.; Zheng, J.; Tang, H. Oxygen evolution reaction kinetics and mechanisms on pristine carbon nanotubes: Effect of pH. *Electrochim. Acta* **2023**, *438*, No. 141146.
(69) Liu, S.; White, M. G.; Liu, P. Mechanism of Oxygen Reduction Reaction on Pt(111) in Alkaline Solution: Importance of Chemisorbed Water on Surface. *J. Phys. Chem. C* **2016**, *120*, 15288–15298.
(70) Liang, Q.; Brocks, G.; Bieberle-Hütter, A. Oxygen evolution reaction (OER) mechanism under alkaline and acidic conditions. *J. Phys. Energy* **2021**, *3*, No. 026001.

Downloaded from pubs.acs.org/aaemcq/article-pdf/9/17/11659/6792706/ae-2026-01791j.pdf by UNIV DEGLI STUDI DI FIRENZE user on 14 September 2026

https://doi.org/10.1021/acsaem.6c01791
ACS Appl. Energy Mater. 2026, 9, 11659–11668